Aerospace Science and Technology 42 (2015) 80–87

Contents lists available at ScienceDirect

Aerospace Science and Technology

www.elsevier.com/locate/aescte

Liquefying fuel regression rate modeling in hybrid propulsion

J.-Y. Lestrade [a,*], J. Anthoine [a], G. Lavergne [b]

[a] Onera – The French Aerospace Lab, F-31410, Mauzac, France
[b] Onera – The French Aerospace Lab, F-31055, Toulouse, France

ARTICLE INFO

Article history:
Received 12 March 2014
Received in revised form 8 September 2014
Accepted 23 November 2014
Available online 9 January 2015

Keywords:
Hybrid rocket engine
Liquefying fuels
1D modeling
Ultrasound measurement technique
Fuel regression law

ABSTRACT

This paper presents an overview of the main hypotheses and equations which lead to the design of the HYDRES platform, a 1D code developed to evaluate liquefying fuel regression rates in hybrid propulsion and the engine propulsive performances. This code is based on an integral description of the aerothermochemical flow coupled to a one equation model for the liquid film. The validation of this numerical code was performed thanks to the HYCOM facility, a lab-scale hybrid engine instrumented, among others, with ultrasonic sensors to follow the ablation of the fuel grain and hence its instantaneous regression rate. Measurements performed during the hybrid engine firing tests also provide the instantaneous regression law of the oxidizer/fuel pair and experimentally highlight the existence of a regression rate limit.

1. Introduction

The development efforts realized for many years on solid and liquid engines made their use almost exclusive for launcher applications (missiles, commercial launchers, sounding rockets, etc.). However, these two concepts have disadvantages (cost, complexity, safety, reliability, environmental impact, etc.) that strain budgetary, propulsive, environment constraints and hinder the development of new applications such as space tourism, nano-launchers, microgravity experiments or landers. Thanks to its benefits in terms of safety, cost, reliability, environmental impact and performances, hybrid propulsion seems to be a promising candidate to overcome these constraints and to facilitate the development of these new applications [6,1].

Hybrid rockets can be considered half way between solid and liquid technologies. The most common configuration consists of a gaseous oxidizer which flows through a solid fuel grain and burns with the pyrolysis gases resulting from the solid fuel regression to form a turbulent and reactive boundary layer. The convective and radiative heat fluxes stemming from the diffusion flame provide the energy needed for the solid grain pyrolysis in order to sustain the heterogeneous combustion [10]. The design of hybrid rocket engines consequently requires a detailed knowledge of these closely interlinked physical phenomena. 2D and 3D CFD models, based on energy and mass balance at the interface and the treatment of the surface pyrolysis by an Arrhenius law, exist for classical polymeric fuels [2,19,17,4]. However, in the preliminary design process of hybrid rocket engines, when various geometrical configurations and performances are studied, a simpler approach can be useful to reduce the computational cost. 1D numerical tools, such as the Onera code DEPHY [7,18,13,14], are consequently more suitable for this task.

The physical mechanisms occurring in the combustion chamber become more complicated when liquefying fuels are used since they pass into gaseous phase by forming a thin and hydrodynamically unstable liquid layer which is convected, vaporized and atomized. Thanks to their degradation process, liquefying fuels demonstrate an increased fuel regression rate [5]. CFD models developed for polymeric fuels are not adapted to liquefying fuels since, on the one hand, the liquid film formed by the melting of the solid fuel and the atomization process are not considered and, on the other hand, heat and mass transfer phenomena encountered for the two kind of fuels are completely different. A 1D model adapted to liquefying fuel has been developed [8].

The objective of the 1D model is to evaluate the regression rate of these fuels considering only the internal geometry of the fuel grain, the inlet conditions of the gaseous flow (pressure, temperature and mass flow rate) and the thermophysical properties of the oxidizer and fuel. Because of the complexity of the physical phenomena involved in the degradation process of these fuels (heat and mass transfers, atomization, combustion, surface regression etc.), the model development was divided in two parts. The first one consisted in modeling the regression rate for a 2D planar and non-reactive flow and validating this model thanks to the HYCARRE

* Corresponding author.
E-mail addresses: jean-yves.lestrade@onera.fr (J.-Y. Lestrade), jerome.anthoine@onera.fr (J. Anthoine).

http://dx.doi.org/10.1016/j.ast.2014.11.015
1270-9638/

Nomenclature

Roman letters

$\dot{m}$	Mass flux	$\mathrm{kg\,m^{-2}\,s^{-1}}$
c_p	Heat capacity	$\mathrm{J\,Kg^{-1}\,K^{-1}}$
v_{reg}	Regression rate	$\mathrm{m\,s^{-1}}$
c	Speed of sound	$\mathrm{m\,s^{-1}}$
E	Entrainment fraction	
h	Thickness	m
P	Pressure	Pa
r	Radial position	m
T	Temperature	K
u	Axial velocity	$\mathrm{m\,s^{-1}}$
x	Axial position	m
Y	Mass fraction	
y	Tangential position	m

Greek letters

α	Thermal diffusivity	$\mathrm{m^2\,s^{-1}}$
δ	Boundary layer thickness	m
λ	Heat conductivity	$\mathrm{W\,m^{-1}\,K^{-1}}$
μ	Dynamic viscosity	Pa s
ϕ	Diameter	m
ρ	Density	$\mathrm{kg\,m^{-3}}$
σ	Surface tension	$\mathrm{N\,m^{-1}}$
τ	Propagation time	s
τ	Shear stress	Pa

Subscripts

amb	Ambient
atom	Atomized
e	Inviscid flow
g	Gaseous phase
ini	Initial
l	Liquid phase
lg	Liquid–gas interface
melt	Melted
ox	Oxidizer
ref	Reference
s	Solid phase
sat	Saturation
sl	Solid–liquid interface
vap	Vaporized

Superscripts

fu	Fuel
ox	Oxidizer

Adimensional numbers

B	Spalding mass transfer number
Re	Reynolds number
St	Stanton number
*We**	Modified Weber number

facility, a two-dimensional test bench dedicated to characterize regression rates of fuels subjected to a hot and non-reactive gaseous flow [9]. The second step of this modeling, on which the first part of this article is focused, considered a 2D axisymmetric flow with combustion, representative of the flow inside hybrid rocket combustion chambers. The validation of this model, presented in the second part of this article, is achieved thanks to the Hycom facility, an instrumented lab-scale hybrid rocket motor providing the necessary data for the numerical model validation.

2. Model description

Modeling hybrid combustion aims in the first place to determine the regression rate of the solid fuel but also the propulsive performances such as thrust or specific impulse. It is therefore necessary to understand the physico-chemical processes governing this particular case of heterogeneous combustion. The gaseous phase reaction first requires the passage to the gaseous state of the solid fuel and its diffusion through the dynamic boundary layer up to the flame zone. After the engine ignition, a fraction of the heat released from the exothermic reaction is transferred to the solid fuel and allows its melting. The development of the thin liquid film thanks to the melting of the solid fuel thus coexists with its disappearing (atomization and evaporation), the balance between these two processes determines the liquid film thickness (Fig. 1). This cycle ensures the self-sustained combustion resulting in an interdependence of heat and mass transfers between the solid, liquid and gaseous phases. The first part of this paper is dedicated to the description of the methodology for modeling these phenomena governing the regression rate process of liquefying fuels. However, although the model was developed for a 2D axisymmetric flow, for the sake of clarity, all the equations presented in this section are written for a 2D planar configuration.

The modeling of the liquefying fuel regression rate appears quite complex when all physical phenomena are taken into account. Some hypotheses are consequently needed in order to simplify this work:

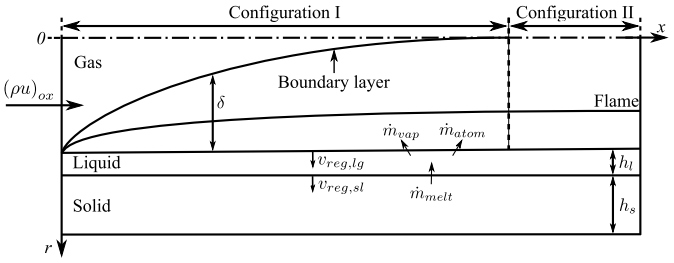

Fig. 1. Modeling configuration.

- Due to the low regression rate values encountered ($\sim$1 mm s^{-1}), the evolution of the fuel grain geometry is slow. The gaseous flow can consequently be considered time independent and an integral method is used to get its mono-dimensional evolution along the combustion chamber. However, although the 1D modeling provides an axial evolution of the fuel regression rate, this rate is assumed uniform along the fuel grain and equal to its averaged value in order to preserve the use of the integral method for modeling the gaseous flow during the regression process.
- The dynamical, the thermal and the chemical boundary layers are supposed to be merged and the kinetic processes of combustion are schematized by an infinitely fast reaction model without radiative transfer.
- Concerning the physical phenomena leading to the atomization of the liquid film developing on the fuel grain, only the atomization process, characterized by an empirical law, is taken into account since a 1D model can not represent hydrodynamic instabilities development nor the dispersed phase in the gaseous flow.

- The solid–liquid interface is supposed to be at the melting temperature of the fuel whereas the liquid–gas interface temperature is equal to its saturation temperature:

$$T_{sl} = T_{melt} \tag{1}$$

$$T_{lg} = T_{sat}(x, P) \tag{2}$$

2.1. Gaseous flow modeling

According to the boundary layer development in a channel, two configurations must be distinguished (Fig. 1). For configuration I, the boundary layer does not fully extend into the channel and an inviscid zone must be treated apart form the boundary layer zone while for configuration II, the boundary layer is fully developed and the confined fluid obeys a Poiseuille flow. However, the second configuration is encountered only for a high L/D ratio and consequently, was not modeled in this study.

Since velocity gradients condition heat and mass transfers, an aerothermochemical model based on an integral description of the flow in the combustion chamber seems the right choice to formulate the gaseous phase. The boundary layer integral method consists in integrating all the transport equations along the normal direction of the fuel grain in a similar way as the one presented by Pelletier and Maisonneuve [13]. The gaseous flow in configuration I requires a separate analytical treatment for both the perfect fluid flow and the boundary layer. The first leads to the integration of mass, momentum, energy through total enthalpy and species conservation equations between the dynamic boundary layer edge and the central channel axis. The second leads to the integration of continuity and momentum equations between the liquid layer and the dynamic boundary layer edge. The introduction of the integral displacement and momentum thicknesses in the last two equations can then link the inviscid flow with the parietal one. Including the perfect fluid relation, all these previous equations represent the perfect gaseous flow and can be written under the following matrix form:

$$A \cdot X' = B \tag{3}$$

with A a 5×5 matrix whose terms are only function of the thermodynamic data in the inviscid flow, B a vector corresponding to the boundary conditions represented by parietal thermodynamical data at the liquid–gas interface and X' the unknown vector defined by:

$$X' = \frac{d}{dx}\begin{bmatrix} u_e \\ \rho_e \\ \delta \\ T_e \\ P \end{bmatrix} \tag{4}$$

The species mass fraction and the total enthalpy do not appear in the unknown vector X' since their longitudinal gradients are null in the inviscid fluid flow.

In order to solve the matrix system, two closure relations have to be added. The first one expresses the velocity profile inside the boundary layer. Since parietal mass injection improves the laminar–turbulent transition, the dynamic boundary layer is considered turbulent all over the channel and the longitudinal velocity is represented by a 1/7 profile according to the gaseous Reynolds number (Eq. (5), Fig. 1)

$$\frac{u_g(r)}{u_e} = \begin{cases} \left(\frac{r_{lg}-r}{\delta}\right)^{1/7} & \text{if } r_{lg} - \delta \le r \le r_{lg} \\ 1 & \text{if } r \le r_{lg} - \delta \end{cases} \tag{5}$$

The second closure relation expresses the friction factor (Eq. (6)) in which the blowing of the liquid–gas interface is taken into account thanks to the Marxman blocking coefficient (Eq. (7)) [11]:

$$\frac{Cf}{2} = \frac{0.296}{Re_x^{0.2}} \cdot \frac{St}{St_0} \tag{6}$$

$$\frac{St}{St_0} = \left[\frac{\ln(1+B)}{B}\right]^{0.8}\left[\frac{1 + 1.3\,B + 0.364\,B^2}{(1+\frac{B}{2})^2(1+B)}\right]^{0.2} \tag{7}$$

with B the mass transfer number which is equal, since the blowing of the liquid–gas interface is similar to the one encountered in droplet evaporation studies, to:

$$B = \frac{Y_{g,lg}^{fu} - Y_g^{fu}}{1 - Y_{g,lg}^{fu}} \tag{8}$$

Finally, the combustion process is represented by the Schwab–Zel'dovich formulation with the Burke–Schumann approximation (infinitely fast chemical reaction). In this case, the flame is located where the gaseous mixture is in stoichiometric proportions and the flame temperature is deduced from an adiabatic flame temperature calculation.

2.2. Liquid film modeling

Due to the small thickness of the liquid film developing along the solid fuel grain ($h_l \sim 10^{-5}$), this layer can be described by a one equation model. This model, valid for Reynolds number based on the liquid film thickness below 100, supposes the local equilibrium of this layer where the inertial forces are neglected. The integral mass conservation equation (Eq. (9)) is the only equation to be resolved where the liquid film thickness is the unknown. Therefore, all terms of this equations have to be related to this thickness:

$$\frac{d\rho_l \overline{u_l} h_l}{dx} = \dot{m}_{melt}\left(1 - \frac{\rho_l}{\rho_s}\right) - \dot{m}_{vap} - \dot{m}_{atom} \tag{9}$$

Thanks to the thin liquid layer hypothesis, the momentum conversation equation can be written as:

$$\mu_l \frac{d^2 u_l}{dx^2} = \frac{dP}{dx} \tag{10}$$

which, once integrated using the adhesion of the liquid film on the solid fuel and the equality of the shear stress at the liquid–gas interface, links the cross-average liquid film velocity to its thickness:

$$\overline{u_l} = -\frac{1}{3\mu_l}\frac{dP_g}{dx}h_l^2 + \frac{\tau_{g,lg}}{2\mu_l}h_l \tag{11}$$

2.3. Mass transfer term modeling

The resolution of the previous equations in the gaseous flow and in the liquid film requires the modeling of the mass transfer terms through the two interfaces. These terms express the vaporized mass flux and the atomized mass flux through the free surface of the liquid layer and the melting mass flux at the solid fuel wall.

The vaporized mass flux is determined by the resolution of the gaseous fuel species in a similar way as in droplet evaporation studies. This source term is consequently expressed as a function of the Spalding mass transfer number defined by Eq. (8).

The atomization process occurring at the free surface of the liquid layer is represented by Sawant's empirical correlation [16] which connects the atomized mass flux to the overall liquid mass flux through the entrainment fraction:

$$E = \left(1 - \frac{250\ln(Re_l) - 1265}{Re_l}\right) \cdot \tanh\left(2.31 \cdot 10^{-4} Re_l^{-0.35} We^{*1.25}\right) \quad (12)$$

with

$$We^* = \frac{\rho_g u_g^2 D_h}{\sigma}\left(\frac{\rho_l - \rho_g}{\rho_g}\right)^{1/3} \quad (13)$$

Finally, the melting mass flux is expressed by resolving the energy conservation in the liquid layer:

$$\frac{d\rho_l c_{p,l} \overline{u_l} \overline{T_l} h_l}{dx} = \lambda_s \left.\frac{\partial T_s}{\partial y}\right|_{sl} - \lambda_g \left.\frac{\partial T_g}{\partial y}\right|_{lg} + \alpha \dot{m}_{melt} + \beta \dot{m}_{evap} + \gamma \dot{m}_{atom} \quad (14)$$

with α, β and γ coefficients depending on thermophysical properties of the liquid.

This equation therefore connects the melting mass flux to the liquid film thickness. However, to solve this equation, three terms have to be modeled. The first one corresponds to the temperature profile in the liquid film. Since its thickness is smaller than the macroscopic length of the flow, the liquid film temperature is assumed to be in equilibrium. Consequently, this data evolves following a linear profile within the liquid layer:

$$T_l(y) = T_{sl} + \frac{T_{lg}(x) - T_{sl}}{h_l}(y_{sl} - y) \quad (15)$$

and the cross-average liquid temperature is therefore equal to:

$$\overline{T_l}(x) = \frac{1}{2}(T_{sl} + T_{lg}) \quad (16)$$

The two other terms to be modeled to solve Eq. (14) are the gaseous thermal flux at the free liquid surface and the solid flux at the melting surface. The first is expressed by the Chilton–Colburn analogy [15] whereas the latter comes from the heat equation in the solid fuel. Considering the solid fuel as a semi-infinite part, this equation provides the temperature profile in the grain:

$$T_s(y) = T_{amb} + (T_{sl} - T_{amb}) \exp\left[\frac{\dot{m}_{melt} c_{p,s}}{\lambda_s}(y - y_{sl})\right] \quad (17)$$

The thermal flux is then expressed by Eq. (18) which relates this thermal flux to the melting mass flux:

$$\lambda_s \left.\frac{dT_s}{dy}\right|_{sl} = c_{p,s}(T_{sl} - T_{amb})\dot{m}_{melt} \quad (18)$$

2.4. Hydres numerical code

The construction of the previous model led to the development of the Hydres (HYbriD Rocket Engine Simulation) platform. The inputs are the oxidizer-fuel pair, the inlet conditions for the gaseous phase and the geometry of the fuel grain. Once the computation is finished, the fuel grain geometry is updated from the averaged regression rate and a new computation is performed at the next time step. The Hydres platform then provides the longitudinal evolution of the thermodynamic data (pressure, velocity, etc.) as well as the temporal evolution of the fuel regression rate and the propulsive performances (specific impulse and characteristic velocity). The instantaneous regression law (Eq. (19)) can then be deduced from these outputs:

$$v_{reg} = a(\rho u)^b \quad (19)$$

The validation of this numerical code is relatively complex. The high level of coupling between all equations previously presented does not allow to find test cases that can be solved analytically. Parts of the code (not involving all the coupling) were however validated with simple test cases and qualitatively coherent data were obtained. The final verification of the code and the quantitative validation of the models can only be done through experimental tests specifically dedicated to this application.

3. Experimental validation of the Hydres numerical code

The experimental validation of the Hydres numerical code was finally performed in two steps, without and with combustion, using respectively two test benches. The first, the Hycarre facility, is a 2D planar test bench dedicated to the characterization of regression rates of fuels subjected to a hot and non reactive gaseous flow [9]. The experimental results obtained on this facility were used to fit Sawant's empirical correlation (Eq. (12)) in order to fit the numerical regression rates with the experimental data. The empirical correlation, developed for precised gaseous–liquid couple, was thus adjusted to the liquefying fuel used during this study and the new correlation (Eq. (20)) was used for all simulations, including those with combustion, without any further modifications.

$$E = 5 \cdot 10^5 \left(1 - \frac{250\ln(Re_l) - 1265}{Re_l}\right) \tanh\left(800 Re_l^{-0.35} We^{*1.25}\right) \quad (20)$$

The second test bench is the Hycom facility, a lab-scale hybrid rocket motor.

3.1. Regression rate measurement technique

To follow the ablation of the fuel grain and hence its instantaneous regression rate, the two facilities were instrumented with ultrasonic sensors. The principle of the ultrasound technique is similar to that of a sonar. An ultrasonic transducer emits a mechanical wave that travels through the tested materials, reflects on the burning surface and travels back to the transducer. The measurement of the wave propagation time is related to the material thickness via the mechanical wave velocity. If the wave velocity is constant, the thickness is proportional to the propagation time:

$$\tau = \frac{2.h}{c} \quad (21)$$

However, the wave velocity evolves with the material temperature (initial value and temperature profile) and with the stress-strain distribution due to the inner pressure and can be expressed as follow:

$$\frac{c_{ref}}{c} = \left(1 + k_T(T - T_{ref})\right)\left(1 - k_P(P - P_{ref})\right) \quad (22)$$

with X_{ref} the reference conditions and k_T and k_P respectively the sensitivity coefficients to the temperature and to the pressure.

In order to take into account the wave velocity evolution in the material, the propagation time has to be written as follow:

$$\tau(t) = 2\int_0^{h_s(t)} \frac{1}{c(y)} \cdot dy \quad (23)$$

Then, due to the hardness of the paraffin-wax used in this study, the stress field is assumed quasi-constant in the material and consequently, the pressure dependency in the relation (22) is neglected ($k_P = 0$). Consequently, thanks to the analytical expression of the temperature profile in the fuel grain (Eq. (17)), the propagation time in the solid phase can be expressed by:

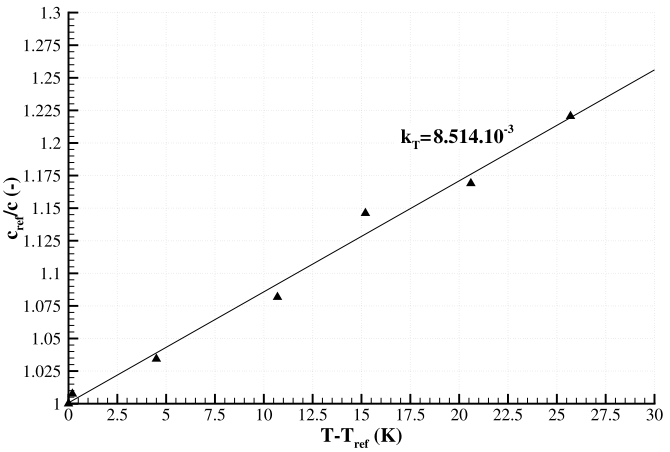

Fig. 2. Speed of sound law of the paraffin-wax.

$$\frac{1}{2}c_{ref}\tau(t) = h_s(t)\left[1 + k_T(T_{amb} - T_{ref})\right] + \frac{k_T\,\alpha_s}{v_{reg}(t)}(T_{melt} - T_{amb}) \cdot \left[1 - \exp\left(-\frac{v_{reg}(t)}{\alpha_s}h_s(t)\right)\right] \quad (24)$$

in which, the solid fuel thickness and the fuel regression rate are related by

$$v_{reg}(t) = \frac{dh_s(t)}{dt} \quad (25)$$

The Onera acquisition system related to the ultrasound measurement technique is based on A-scan storage at a high repetition rate for each channel. Thanks to a post-processing analysis, a discrete evolution of the propagation time is then derived by determining the position, as a function of the time, of the maximum positive amplitude data of the useful pulse. To obtain the fuel regression rate from Eqs. (24) and (25), these ones are therefore discretized and solved numerically by a Newton method. The constants k_T and c_{ref} appearing in Eq. (24) are then determined experimentally by performing discrete measurements of the travel time on a fuel sample of calibrated thickness for precise temperatures. As presented in Fig. 2, the evolution of the adimensional speed of sound as a function of the temperature rise is almost linear and in agreement with relation (22) in which $k_P = 0$ since, for the paraffin-wax used, this law is expressed by

$$\frac{2554}{c(T)} = 1 + 8.514 \cdot 10^{-3}(T - 293.15) \quad (26)$$

3.2. Description of the Hycom facility

The Hycom facility (Fig. 3) is a lab-scale hybrid engine dedicated to the instantaneous fuel regression rate measurement in order to validate the Hydres numerical code. Like most hybrid rocket motors, the Hycom engine is composed of five parts (Fig. 4): a forward end-plate including the injector, a pre-chamber including the igniter, a combustion chamber, a post-chamber and a nozzle. This facility was designed, by making the different parts modular, to easily change the lengths of the pre- and post-chambers, the geometry of the fuel grain, the type of injector, etc. The fuel grain can reach 230 mm for the length and 82 mm for the external diameter. The maximum operating pressure is 7.5 MPa and the engine is instrumented with an oxidizer Coriolis mass flow meter, four pressure probes (two in the pre-chamber and two in the post chamber) and ultrasound sensors (one located at the head-end of the fuel grain and two at the rear-end). The facility is also connected to a thrust sensor in order to measure the thrust.

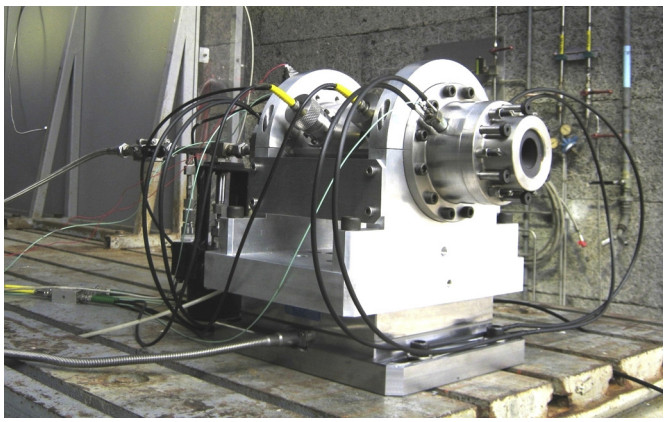

Fig. 3. The Hycom lab-scale hybrid engine.

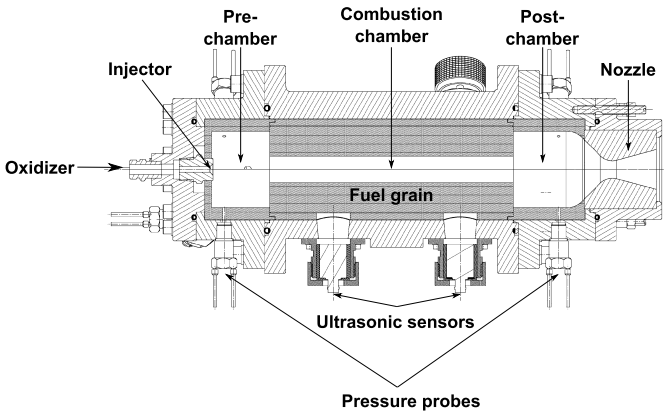

Fig. 4. Schematic view of the Hycom facility.

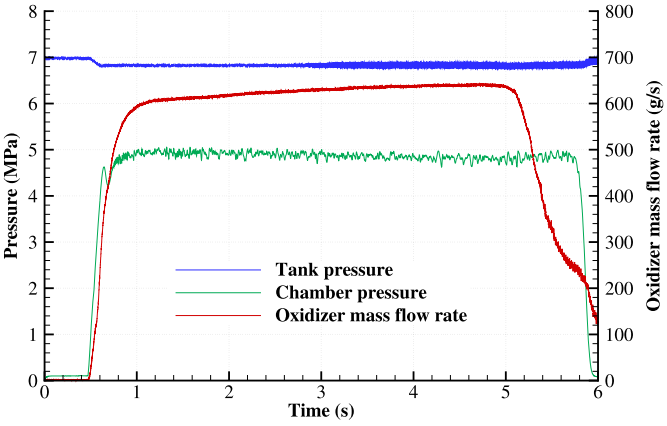

Fig. 5. Reference test results.

Tests were carried out with pressurized N_2O as oxidizer and paraffin-wax as fuel for different operating conditions in terms of initial oxidizer mass flux and chamber pressure in order to determine the influence of these parameters on the fuel regression rate and to have a better validation of the Hydres platform.

3.3. Experimental results

The reference test was performed with an initial diameter of the fuel grain of 27 mm, a fuel length of 230 mm and a conical nozzle with a 16.3 mm throat diameter. As presented in Fig. 5, the tank pressure is constant during the test and close to 7 MPa. Although the oxidizer mass flow rate evolves slightly during the

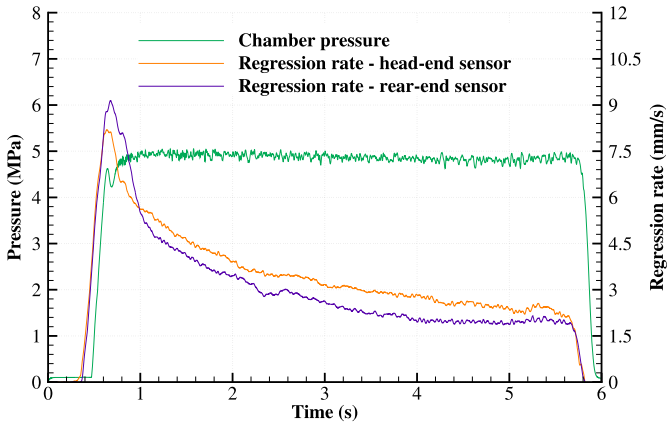

Fig. 6. Instantaneous fuel regression rate for the reference test.

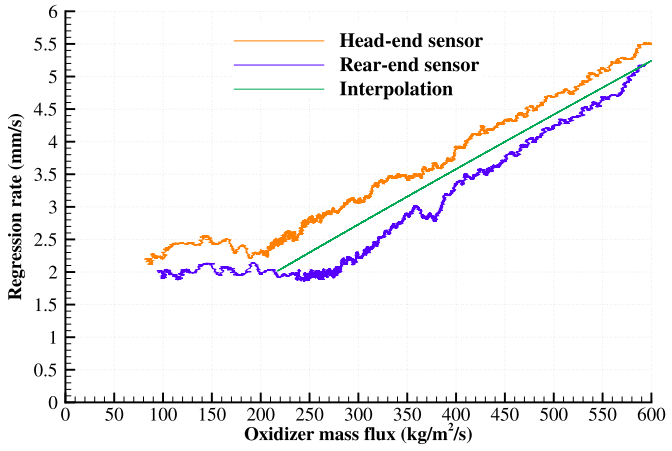

Fig. 7. Instantaneous fuel regression laws for the reference test.

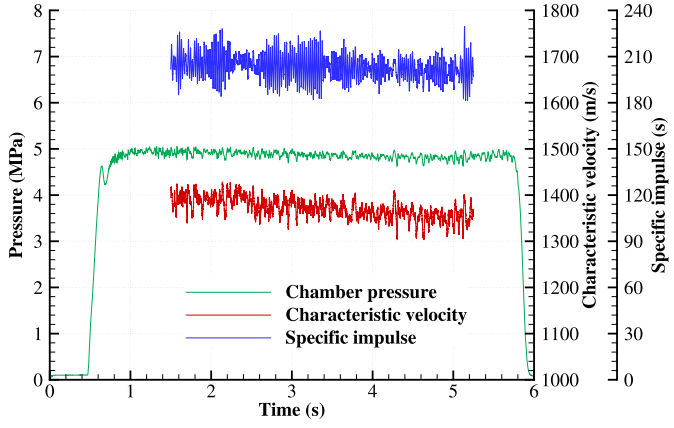

Fig. 8. Instantaneous propulsive performances for the reference test.

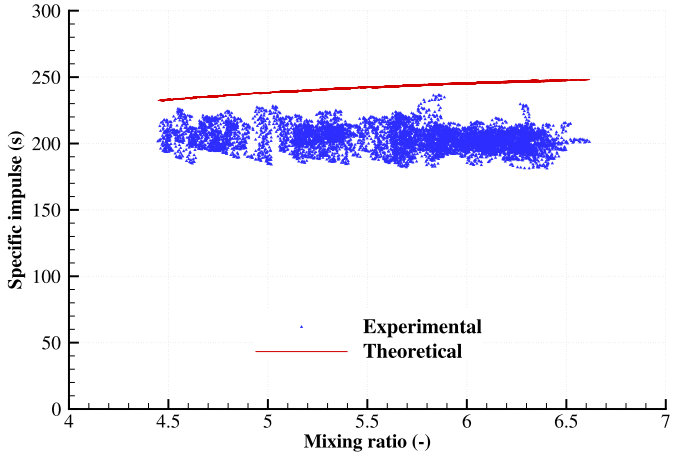

Fig. 9. Evolution of the specific impulse as a function of the mixing ratio for the reference test.

firing test, its value is close to the expected 600 $g\,s^{-1}$ and provides a chamber pressure of about 5 MPa. At the end of the firing test, the nitrous oxide quantity contained in the tank was no longer sufficient to keep the oxidizer liquid and gaseous N_2O was consequently injected in the combustion chamber. As shown in Fig. 5, the chamber pressure remains however constant until the time at which the oxidizer valve was closed (5.8 s). The flow rate data in Fig. 5 have consequently to be discarded after 5.2 s. Data analysis of the ultrasound measurements have enabled to get the instantaneous fuel regression rate at the location of each sensor which evolves between 9 and 2 $mm\,s^{-1}$ during the test (Fig. 6).

The instantaneous oxidizer mass flux is then deduced by combining the evolutions of the oxidizer mass flow rate and of the internal diameter of the fuel grain, output of the ultrasound measurement technique. This data then provides the regression law (Fig. 7) which presents two evolutions. For an oxidizer mass flux greater than 250 $kg\,m^{-2}\,s^{-1}$, the evolution, expressed by Eq. (27), is quasi-linear whereas, below this value, the regression rate is constant and around 2 $mm\,s^{-1}$ even if the oxidizer mass flux decreases. It appears also that the upstream part of the fuel grain deteriorates faster than the downstream section of the solid fuel which is in agreement with the fuel regression law (Eq. (19)) since the oxidizer mass flux decreases along the fuel grain.

$$v_{reg} = 1.28 \cdot 10^{-5} (\rho u)_{ox}^{0.94} \tag{27}$$

The instantaneous fuel regression rate measurement also enables to plot the evolution of the propulsive performances. As presented in Fig. 8, the characteristic velocity and the specific impulse are quite constant during the firing test. The instantaneous specific impulse is then plotted as a function of the instantaneous mixing ratio to compare the experimental evolution with the theoretical one obtained thanks to a thermochemical equilibrium code using the experimental pressure and the mixing ratio as inputs (Fig. 9). The combustion and the rocket efficiencies are therefore deduced from the comparison between the experimental characteristic velocity and specific impulse with their theoretical values. These two efficiencies, respectively 88.5% and 84.5%, are used in the Hydres platform to have a better estimation of the chamber pressure and of the thrust.

Other tests were performed on this facility in order to characterize the influence of different parameters on the regression law (Fig. 10). It appeared that the initial oxidizer mass flux has no influence on the regression rate since the slopes are superimposed and that, as expected, chamber pressure has a second order effect. Therefore, all the experimental regression laws present the same behavior with one part nearly linear and another where the regression rate is almost constant. The existence of this regression rate limit was supposed by Muzzy [12] and Chiaverini [3] for classical polymeric fuels (Fig. 11). According to this author, for small oxidizer mass fluxes, radiative transfers dominate the convective ones and are at the source of this limit value. This theory could be applied for liquefying fuels since, for small oxidizer mass flux, the atomization is negligible and consequently, the degradation process of liquefying fuels is quite similar to that of classical fuels.

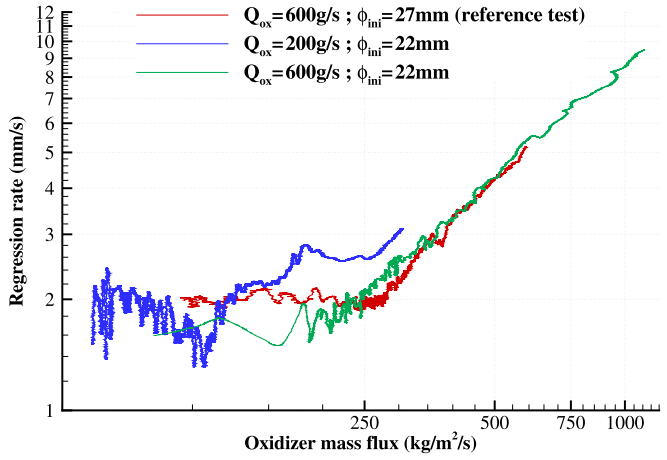

Fig. 10. N_2O/paraffin regression laws from experimental tests performed on the HYCOM facility (rear-end sensor).

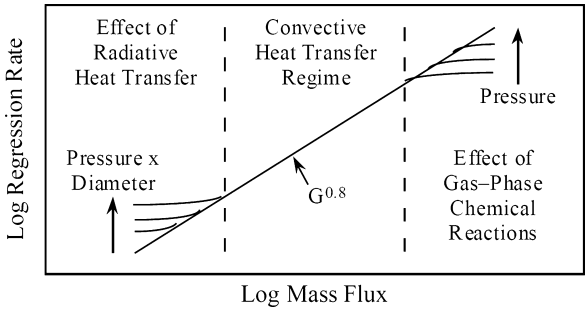

Fig. 11. Muzzy regression law for classical polymeric fuels.

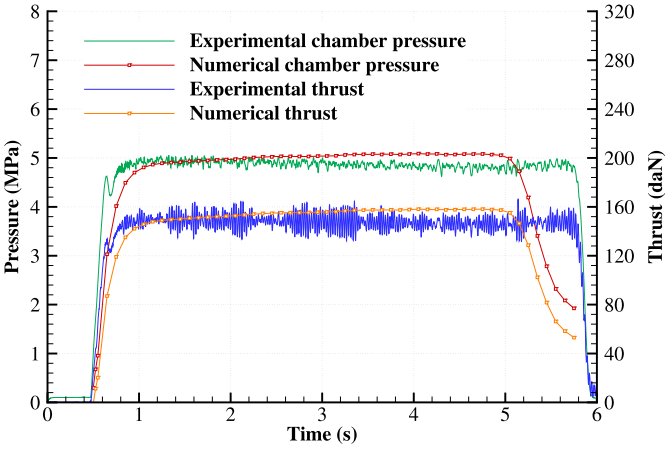

Fig. 12. Experimental/numerical comparison on the HYCOM reference test.

3.4. Numerical/experimental comparison

The simulations performed with the HYDRES numerical code use the evolution of the oxidizer mass flow rate measured experimentally as input. The combustion and rocket efficiencies are also taken into account to have better chamber pressure and thrust evaluation. During the numerical process, the pressure at the first node of the mesh is automatically adjusted in order to respect the thermodynamical equilibrium in the combustion chamber.

As presented in Fig. 12, the experimental evolutions of the chamber pressure and of the thrust are quite well reproduced by the numerical code. The slight difference between the experimental and numerical results comes from the use of constant efficiencies in the numerical code which underestimates the experimental data at the beginning of the test and overestimates them at the end of the test. However, as explained previously, the oxidizer mass flow rate presents a decrease at the end of the firing test (Fig. 5) due to the injection of gaseous nitrous oxide. Consequently, since this data is an input of the HYDRES numerical code, the evolutions of the chamber pressure and of the thrust can not be correctly simulated at the end of the firing test. The average regression laws (Figs. 13 to 15) are nevertheless very well estimated although the model does not reproduce the part where

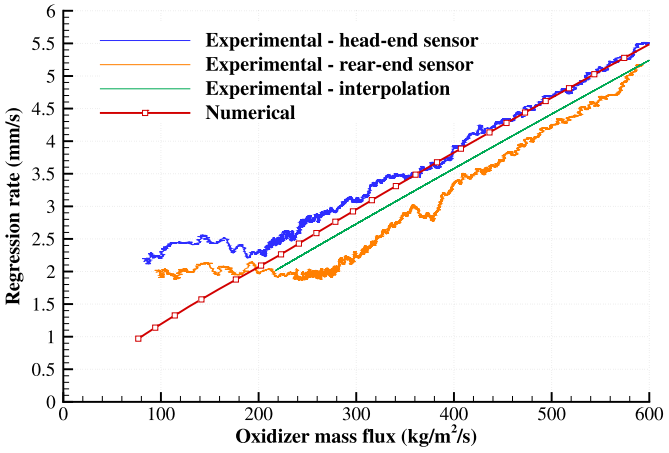

Fig. 13. Comparison of the regression law for the reference test.

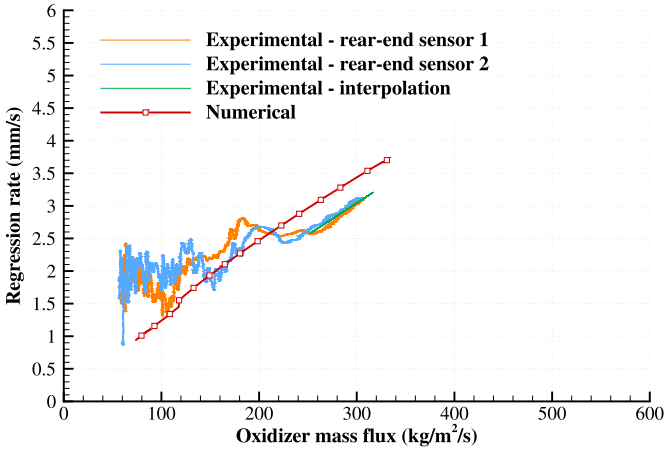

Fig. 14. Comparison of the regression law for the second test.

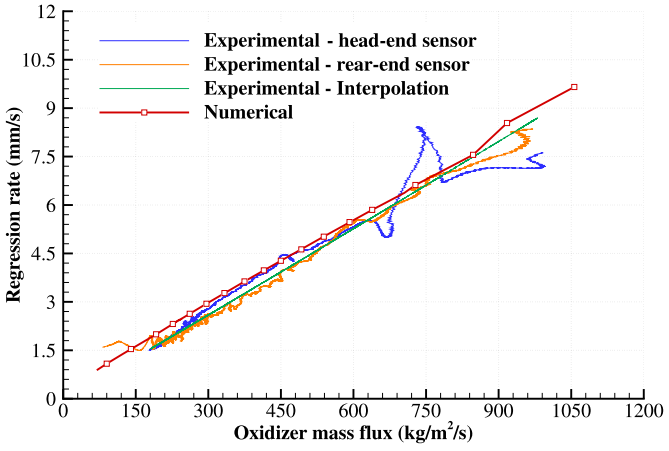

Fig. 15. Comparison of the regression law for the third test.

the regression rate is constant (for oxidizer mass flux lower than 250 $\mathrm{kg\,m^{-2}\,s^{-1}}$).

4. Conclusion

This paper presented the hypotheses and the main governing equations at the origin of the Hydres platform, a 1D numerical code developed to evaluate liquefying fuel regression rates in hybrid propulsion and the engine propulsive performances. This modeling is based on an integral description of the aerothermical flow coupled with a one equation model for the liquid film.

In parallel to this development, tests were performed under different operating conditions on the Hycom facility, a lab-scale test-bench designed and instrumented to provide the data for the numerical model validation. The combination of ultrasonic and oxidizer mass flow rate measurements allows to obtain the instantaneous regression law of the oxidizer/fuel pair under precise operating conditions. It also allows to highlight the existence of the regression rate limit which was supposed by Muzzy but never proved.

Finally, the Hydres platform was validated since the numerical results match the experimental data very well in the validity range of the hypothesis (for oxidizer mass flux higher than 250 $\mathrm{kg\,m^{-2}\,s^{-1}}$).

Conflict of interest statement

None declared.

Acknowledgements

This work was performed through a PhD thesis at Onera supported by CNES (grant number 4500032827/DLA094) and defended in December 2012. The author would like to thanks N. Cesco from CNES for her continuous support to this work.

References

[1] J. Anthoine, Y. Maisonneuve, M. Prevost, The hybrid propulsion to serve space exploration and micro-gravity experiments, in: 61st International Astronautical Congress, Prague, Czech Republic, 2010, iAC-10-C4.6.9.

[2] G.C. Cheng, R.C. Farmer, H.S. Jones, J.S. McFarlane, Numerical simulation of the internal ballistics of a hybrid rocket motor, in: 32nd Aerospace Sciences Meeting & Exhibit, 1994, aIAA Paper 94-0554.

[3] M. Chiaverini, Review of solid-fuel regression rate behavior in classical and non-classical hybrid rocket motors, in: M.J. Chiaverini, K.K. Kuo (Eds.), Fundamentals of Hybrid Rocket Combustion and Propulsion, in: Progress in Astronautics and Aeronautics, vol. 218, 2007, pp. 37–126, Ch. 2.

[4] G. Gariani, F. Maggi, L. Galfetti, Numerical simulation of HTTP combustion in a 2D hybrid slab combustor, Acta Astronaut. 69 (2011) 289–296, http://dx.doi.org/10.1016/j.actaastro.2011.03.015.

[5] M.A. Karabeyoglu, G. Zilliac, B.J. Cantwell, S. De-zilwa, P. Castelluci, Scale-up tests of high regression rate liquefying hybrid rocket fuels, in: 41st AIAA Aerospace Sciences Meeting & Exhibit, 2003, aIAA Paper 2003-6475.

[6] G. Lengelle, Y. Maisonneuve, Hybrid propulsion: past, present and future perspectives, in: 6th International Symposium on Propulsion for Space Transportation of the 21st Century, Versailles, France, 2002.

[7] G. Lengelle, P. Simon, P. Hoc, F. Dijkstra, Design tool for hybrid motors, in: 5th International Symposium for Space Transportation Propulsion, Paris, France, 1996.

[8] J.-Y. Lestrade, Modélisation de la régression des combustibles liquéfiables dans un moteur hybride, PhD thesis, Institut Supérieur de l'Aéronautique et de l'Espace, 2012.

[9] J.-Y. Lestrade, J. Anthoine, G. Lavergne, Liquefying fuel in hybrid propulsion: first step towards a 1D model, in: 4th European Conference for Aero-Space Sciences, St. Petersburg, Russia, 2011.

[10] G.A. Marxman, M. Gilbert, Turbulent boundary layer combustion in the hybrid rocket, Symp., Int., Combust. 9 (1963) 371–383, http://dx.doi.org/10.1016/S0082-0784(63)80046-6.

[11] G.A. Marxman, C.E. Wooldridge, The incompressible, turbulent boundary layer on a flat plate with homogeneous injection, Tm-33-64-u1, United Technology Center, 1964.

[12] R.J. Muzzy, Applied hybrid combustion theory, in: 8th AIAA Joint Propulsion Conference, 1972.

[13] N. Pelletier, Y. Maisonneuve, A numerical code for hybrid space propulsion design & tests, in: 3rd International Conference on Green Propellants for Space Propulsion, Poitiers, France, 2006.

[14] M. Prevost, G. Guillement, Modelling of hybrid rocket motor: 1D regression rate prediction model, in: 4th European Conference for Aero-Space Sciences, St. Petersburg, Russia, 2011.

[15] J.F. Sacadura, Initiation aux Transferts Thermiques, 6th edition, Technique et Documentation, 2000.

[16] P. Sawant, M. Ishii, M. Mori, Droplet entrainment correlation in vertical upward co-current annular two-phase flow, Nucl. Eng. Des. 238 (6) (2008) 1342–1352, http://dx.doi.org/10.1016/j.nucengdes.2007.10.005.

[17] N. Serin, Y.A. Gogus, Navier–Stokes investigation on reacting flow field of HTTP/O2 hybrid motor and regression rate evaluation, in: 39th AIAA Joint Propulsion Conference, 2003, aIAA Paper 2003-4462.

[18] P. Simon, Modélisation et simulation des mécanismes de la combustion hybride dans un système propulsif, PhD thesis, Université de Poitiers, 1996.

[19] S. Venkateswaran, C. Merkle, Size scale-up in hybrid rocket motors, in: 34th Aerospace Sciences Meeting & Exhibit, 1996, aIAA Paper 96-0647.